Strain engineering via amorphization and recrystallization in Si/Ge heterostructures

Yumi Park,[1] Winnie Tan,[1] and Alejandro Strachan[1,2,*]
[1]*School of Materials Engineering, Purdue University, West Lafayette, Indiana 47907, USA*
[2]*Birck Nanotechnology Center, Purdue University, West Lafayette, Indiana 47907, USA*
(Received 28 January 2011; revised manuscript received 21 April 2011; published 6 September 2011)

We use molecular dynamics with the reactive potential ReaxFF to study strain relaxation during the amorphization and recrystallization of silicon-germanium epitaxial nanolaminates. Starting with a coherent heterostructure with (010) Si/Ge interfaces and 3D periodic boundary conditions, we use local heating and quenching to amorphize half of the simulation cell with crystal-amorphous interfaces normal to [001]. We find strain relaxation along [001] as the crystalline Ge section expands into the amorphous material and crystalline Si contracts from it. The amount of strain relaxation correlates with the atomic transport from the amorphized Ge to Si section and increases as the periodic width of the crystalline-amorphous pattern decreases and the height of the Si/Ge bilayer increases. Recrystallization leads to a decrease in strain relaxation; however, structures with low aspect ratio retain a significant fraction of the strain relaxation. Interestingly, this remnant strain relaxation is not due to misfit dislocations but originates in clusters of lattice defects located on either side of the interface and caused by atomic transport. Our results show that local amorphization followed by recrystallization is a possible avenue for strain engineering in semiconductor heterostructures.

DOI: 10.1103/PhysRevB.84.125412 PACS number(s): 62.25.−g, 68.35.Gy, 62.40.+i, 81.40.Jj

I. INTRODUCTION

Nanoscale heterostructures are ubiquitous in a wide range of applications, including electronic, optoelectronic, and energy conversion devices.[1–3] The ability to design and fabricate nanostructures with engineered complexity (e.g., specific levels of multiaxial strain and interfaces with low-defect densities) is critical in the development and optimization of next-generation devices with improved properties.[4] Strain is an effective avenue to engineer new or improved functionalities in nanoscale materials, including electronic properties arising from band structure modification,[1] ferroelectricity,[5] and thermal conductivity.[6] In the case of electronic properties of interest here, an anisotropic strain state breaks the symmetry of cubic semiconductors, reshaping their band structures. Uniaxially strained Si channels lead to performance improvement in conventional Si n-MOSFET by enhancing electronic mobility.[7,8] Also, strain engineering in Ge has been investigated experimentally[9] and theoretically[10] since uniaxially strained Ge is desirable for p-MOSFET because of its high hole mobility. In this paper, we focus on strain engineering in Si/Ge epitaxial nanolaminates via local amorphization and recrystallization using molecular dynamic (MD) simulations. We find that for certain geometries, local amorphization relaxes the initial biaxial strains in the crystalline sections of the nanolaminates along the direction normal to the amorphous-crystalline interface because the crystalline Ge region expands into the amorphized section and Si contracts from it. As mentioned earlier, such strain states are desirable for some applications in the semiconductor industry,[11] and, in agreement with recent experiments,[12] our simulations show that local amorphization can be a useful technique for strain engineering. We here quantify how size and geometry affect strain relaxation and the effect of recrystallization. Interestingly, we find that for low-aspect-ratio geometries, some of the strain relaxation is retained even after recrystallization, but it is also possible to design geometries for which the original state of biaxial strain of the nanolaminate is recovered after recrystallization. These last geometries should be used in devices in which the desired multiaxial strain is engineered before amorphization by ion bombardment.[8]

II. SIMULATION DETAILS

A. Interatomic potential

We used the reactive potential ReaxFF parameterized for Si based on extensive *ab initio* calculations developed in van Duin *et al.*[13] and refined in Buehler *et al.*[14] ReaxFF uses the concept of partial bond order to describe covalent bonding in Si and has been parameterized to describe the equation of state of various phases of Si (with different coordination numbers), as well as angle bending and Si-Si bond breaking processes in various small molecules.[13] Because of its ability to describe bond breaking and formation, ReaxFF has been successfully used to describe the process of crack propagation,[13] brittle-to-ductile transition in Si at elevated temperatures,[15] and strain relaxation in nanoscale bars.[10] An accurate description of high-energy conformations in which atoms experience environments very different from that in the bulk is critical for the application of interest here that involves crystalline and amorphous regions, as well as large strains near interfaces. To describe the interactions between Ge atoms, we simply generate force field parameters by increasing all the distance parameters of Si by a factor of 1.0417—the ratio of lattice parameters between Ge and Si. Also, the van der Waals cross-interactions between Si and Ge are characterized by using Si parameters. This Si/Ge potential predicted strain relaxation in strained Si/Ge/Si nanobars in good agreement with experimental measurements.[10]

B. Initial Si/Ge heterostructures

Figure 1(a) shows an atomic snapshot of one of the initial Si/Ge nanolaminates. To build these heterostructures, we start with the cubic unit cell of the diamond crystal structure and

 ©2011 American Physical Society

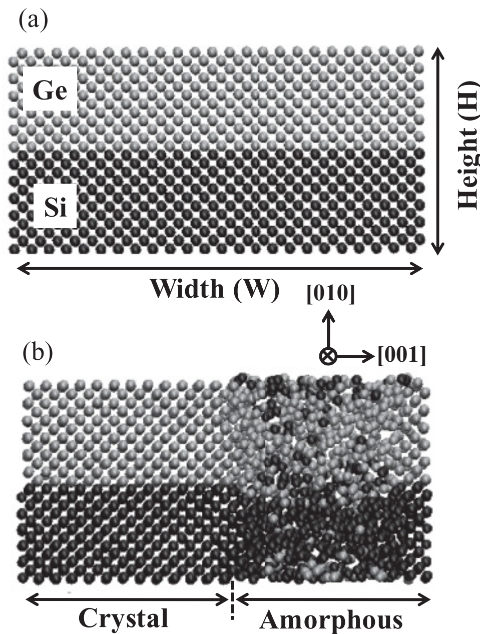

FIG. 1. Snapshots of Si/Ge heterostructure (a) before and (b) after amorphization.

replicate it to generate structures with various widths (W) in the [001] direction and heights (H) along [010]. In all cases, the unit cell is replicated five times in the [100] direction, and periodic boundary conditions are imposed in all three directions. The atoms in the bottom half of the unit cells along [010] are Si, and the remaining atoms are Ge. Because of the lattice mismatch, both Si and Ge are biaxially strained on the (010) plane (the plane parallel to the Si/Ge interface), but there is no stress in the direction normal to the interfacial plane. Consequently, the lattice parameters of the Si and Ge sections along [100] and [001] are identical because of the epitaxial character of the heterostructures (as long as the system remains crystalline and retains coherent interfaces). For all our simulations, we keep the simulation cell lengths along [100] and [001] constant at $a_x = a_z = 5.428\,44$ Å; the strains of Si and Ge along these directions are 2% and −2.09%, respectively, using ReaxFF lattice parameters. These in-plane lattice parameters are chosen to reproduce what one would achieve experimentally in Si/Ge epitaxial films on virtual substrates.[9] On the other hand, the nanostructure is free to relax along the [010] direction (normal to the Si/Ge interface). Thus, we optimized the simulation cell length along this direction by minimizing the internal energy. The obtained value (a_y) is 5.408 74 Å, leading to strains of 1.63% and −3.60% for Si and Ge, respectively. This MD result is in good agreement with the prediction of linear elasticity theory for biaxially strained heterostructure

$$\varepsilon_{yy} = -2 \cdot \varepsilon_{xx} \cdot \upsilon/(1-\upsilon), \tag{1}$$

where $\upsilon_{\text{si}} = 0.33$ and $\upsilon_{\text{Ge}} = 0.22$ are the Si and Ge Poisson's ratios for ReaxFF. The average lattice parameter along [010] (a_y) is 5.4135 Å, but we stress that the Si and Ge sections have different lattice parameters.

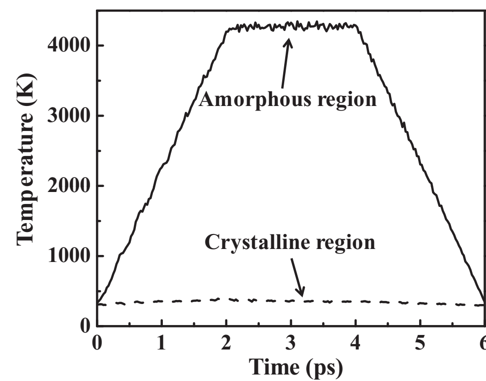

FIG. 2. The temperature profile of Si/Ge heterostructure during annealing. Only half of the structure is annealed at 4300 K for local amorphization.

C. Amorphization and recrystallization procedure

To create an amorphous region, we melt and quench approximately half of the system. To achieve this, we divide the system in halves along [001] and use a MD procedure consisting of three stages to amorphize one of the resulting regions: (i) The temperature of half of the system is rapidly heated to $T = 4300$ K within 2 ps, whereas the other half is kept at $T = 300$ K. (ii) These temperature conditions are maintained for an additional 2 ps. (iii) Finally, the hot region is cooled down to $T = 300$ K in 2 ps. To control the temperature, a Berendsen thermostat[16] with a damping constant of 100 fs was used in our MD simulations. Figure 2 shows temperature as a function of time in the crystalline ($T = 300$ K) and amorphous regions during the heating and cooling procedures. As a result of this procedure, a locally amorphized Si/Ge heterostructure is generated, as shown Fig 1(b). The extremely fast heating and cooling rates are designed to minimize interdiffusion of Si and Ge atoms, as would be expected in experiments in which amorphization is achieved by ion bombardment. The simulation cell parameters are kept constant during the amorphization and recrystallization procedures to mimic the mechanical constraints caused by other regions of material surrounding the locally amorphized area on the devices.

D. Structural analysis of MD simulations

We compute local strains along [100], [010], and [001] in the Si and Ge sections of our heterostructures using the following procedure. We first calculate the distance between every pair of first nearest neighbor atoms and project this vector along each of the Cartesian axes. To obtain local strain profiles along [001] (normal to the amorphous/crystalline interface), the heterostructures are divided into bins of width 1.331 Å (1/4 of the lattice parameter) and the projected bond distances in each bin are averaged over a period of 10 ps. Strains on Si and Ge are calculated using these average projected bond distances and those of the unstrained crystals: 1.331 Å for Si and 1.386 Å for Ge. Note that this calculation does not provide a measure of strain in the amorphous regions, and the projected bond distances will be smaller because of random orientation of the bonds.

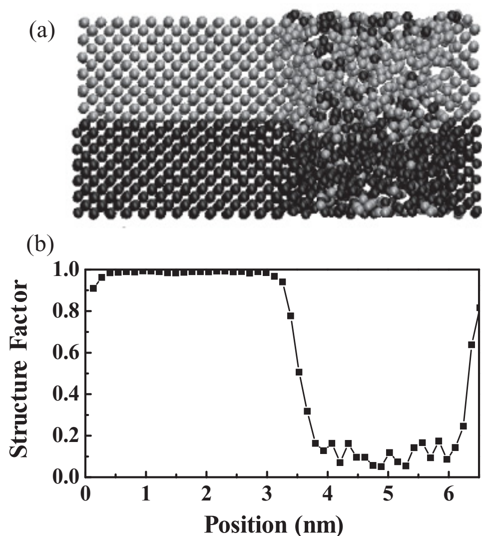

FIG. 3. Structure factor (b) of a locally amorphized Si/Ge nanolaminate (a). Crystalline region shows a structure factor near one, and the amorphous region leads to values close to zero.

The amorphous/crystalline interfaces and recrystallization velocities are identified by computing the local structure factor defined as[17]

$$S_i(z) = \left| \frac{1}{N_i} \sum \exp[ik_x \cdot r_{ij}] \right|, \qquad (2)$$

where z and $k_x = 8\pi/a_x$ are the interface growth direction and the reciprocal lattice vector parallel to the x direction, respectively. Each structure is divided into slices with the same width of 1.357 Å (i.e., 1/4 of the 2% strained lattice parameter) along the interface growth direction (z) for the calculation. N_i is the number of atoms in the ith slice, and $r_{ij} = (x_j, y_j, z_j)$ represents the atomic position of atom j in the ith slice. The structure factor in the crystalline region is close to 1, but it approaches 0 when the structure looses long-range order. Figure 3 shows the structure factor as a function of position along the z direction for a locally amorphized sample; as expected, the structure of the amorphous region is smaller than that of the crystal, and the two interfaces can be clearly identified.

III. STRAIN RELAXATION IN CRYSTALLINE/ AMORPHOUS STRUCTURES

Figure 4 shows the average projected bond distance for Si and Ge atoms as a function of position along the [001] axis for three structures with different geometries. We see that the crystalline Ge region can expand into the amorphous material, whereas Si contracts from it, leading to strain relaxation along [001]. Figure 4 also shows that strain relaxation increases with decreasing width (W) of the amorphous/crystalline regions and with increasing bilayer height (H). For the highest aspect ratio case, Fig. 4(c) with $W = 13.03$ nm and $H = 3.25$ nm, Si and Ge have the same lattice parameter throughout most of the crystalline region, leading to little strain relaxation. The local relaxation is more important as the ratio between the width and height (W/H) decreases: the structure in Fig. 4(a), with a lower aspect ratio of 0.84, exhibits significant strain relaxation of

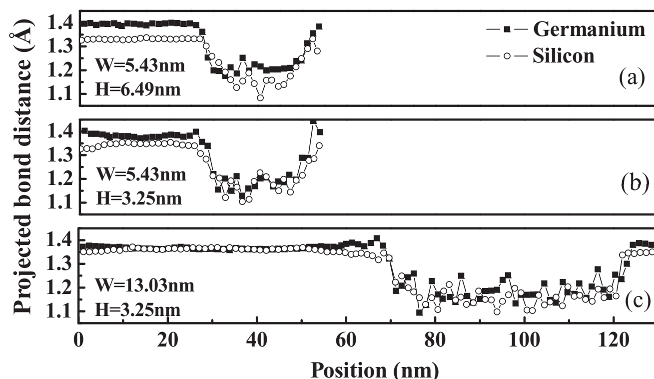

FIG. 4. Projected bond distance as a function of position for three structures with different aspect ratios: (a) 0.84, (b) 1.67, and (c) 4. As the aspect ratio (*W/H*) decreases, Si and Ge relax in the direction normal to the amorphous/crystal interface releasing the initial biaxial strain.

~113.51%. The mechanisms responsible for strain relaxation and its dependence on width and height will be discussed in detail in Sec. V.

IV. RECRYSTALLIZATION AND STRAIN EVOLUTION

To characterize the role of recrystallization on strain relaxation, we annealed the amorphized Si/Ge heterostructures at various temperatures until each structure was fully recrystallized. The lower free energy of the crystal drives recrystallization, as can be seen in Figs. 5(a)–5(c), where we show atomic snapshots and structure factor profiles of the process at $T = 2000$ K. For this high temperature, the amorphous region is fully recrystallized after 1.5 ns. The snapshot in Fig. 5(c) shows that the recrystallized structure is coherent except for atomic substitutional disorder arising from initial Si/Ge interdiffusion.

A. Temperature dependence of recrystallization velocity

Besides the characterization of strain relaxation, the recrystallization simulations provide an opportunity to validate the accuracy of our approach because accurate experimental measurements of recrystallization velocity as a function of temperature are available for Si and Ge.[18] In solid-phase epitaxy (SPE) of Si, the velocity (or SPE rate) of the crystalline-amorphous interface can be described by an Arrhenius equation defined as $v = v_0 \exp[-E_a/kT]$. Where, v_0, E_a, T, and k represent the pre-exponential factor, activation energy, temperature, and Boltzmann constant, respectively.[18] We use the structure factor profiles to indentify the location of both amorphous/crystalline interfaces, where $S(z) = 0.5$, at various times, and from this information, we compute the interface velocity for various temperatures. Figure 6 shows the average recrystallization velocity of the two solid-amorphous interfaces as a function of inverse temperature obtained from our simulations. Experimental data on amorphous Si (a-Si) interfacial velocity in the temperature range from ~743 K to ~1623 K shows an Arrhenius behavior with $E_a = 2.8$ eV.[18] For amorphous Ge, E_a obtained over the temperature range 573 K to ~813 K is 2.15 eV.[19] Extrapolations of these experimental

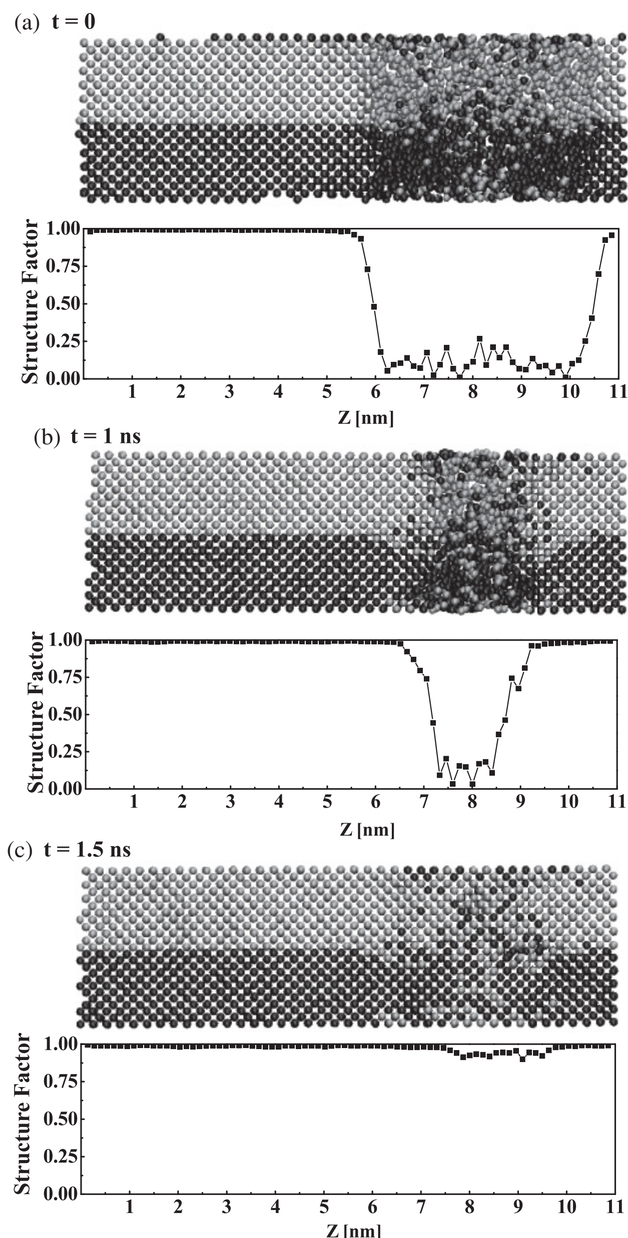

FIG. 5. Structure factor (SF) along the SPE growth direction for (a) $t = 0$ ns, (b) $t = 1$ ns, and (c) $t = 1.5$ ns. Such profiles are used to identify the amorphous/crystalline interfaces at different times and compute their velocities.

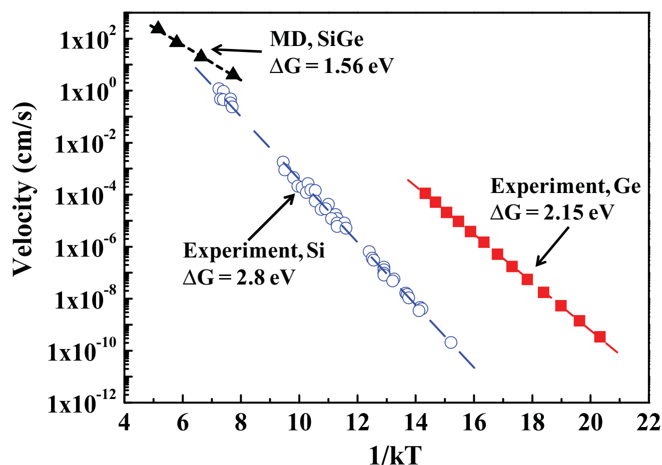

FIG. 6. (Color online) Recrystallization velocities for Si/Ge nanolaminates (triangles) as a function of inverse temperature in an Arrhenius plot. The fit (dashed line) gives an activation energy of 1.56 eV. Circles (Olsen and Roth[18]) and squares (Johnson *et al.*[19]) are the SPE rates obtained experimentally for Si and Ge, respectively.

results are shown as dashed lines in Fig. 6. The recrystallization velocities from MD also show an Arrhenius temperature behavior for our Si/Ge laminates with velocities comparable to experiments in Si and Ge, and activation energy in Si/Ge is 1.56 eV, lower than the experimental values for Si and Ge. These results are comparable with the current state of the art atomistic predictions, and several factors can contribute to this difference, including size effects, simulation cell lengths that are kept constant throughout the simulations, limitations of the interatomic potential, and the Si/Ge laminate internal strains of our simulations. Krzeminski *et al.*[20] obtained the Si activation energy of 1.85 eV using a newly parameterized Stillinger–Weber potential (SW115),[21] and Posselt *et al.*[22] obtained an activation energy of 1.09 eV for Ge using Stillinger–Weber. For both cases, the activation energies are underestimated, and the absolute values of velocities are slightly higher than the experiments.[18,19] Cleri *et al.*[20] also reported that the Tersoff potential, predicting an activation energy of 2.99 eV, leads to better agreement with the experimental results for Si, whereas the original Stillinger–Weber potential and the environment-dependent interatomic potential (EDIP) seem to be unable to describe the amorphous-to-crystal solid-solid transitions accurately.

B. Role of recrystallization on strain relaxation

After complete recrystallization of the Si/Ge structures at $T = 2000$ K, we performed a 50-ps-long constant volume and temperature MD simulation (NVT ensemble) at $T = 300$ K to thermalize the system and then calculated strain, averaging configurations over the final 10 ps of these runs. Figure 7 shows the average projected bond distance for two structures recrystallized with different aspect ratios. For the structure with $W = 5.43$ nm and $H = 3.25$ nm ($W/H = 1.67$) [Fig. 7(a)], our simulations predict essentially the same lattice parameters for Si and Ge. That is, in this case, the strain relaxation is lost during recrystallization and the original state of biaxial strain is recovered. We also observe small variations in the lattice parameter in the recrystallized region because of some intermixing of Si and Ge atoms, as shown in Fig. 8(a). For a smaller aspect ratio nanostructure, Fig. 7(b) shows that for $W = 5.43$ nm and $H = 6.49$ nm ($W/H = 0.84$), the crystalline region retains some of the strain relaxation achieved during amorphization, even after full recrystallization. The atomistic snapshot in Fig. 8(b) reveals the interesting atomic origin of this phenomenon. We find clusters of point defects in the recrystallized Si and Ge regions. This is a surprising result since strain relaxation in heterostructures is typically due to misfit dislocations at interfaces, and we observe strain relaxation with perfectly coherent interfaces. Likely reasons for this observation are that the small size of the nanostructures

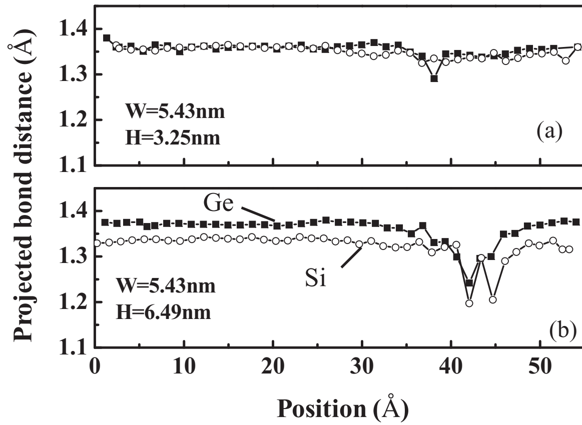

FIG. 7. Projected bond distances along the [001] direction for structures with different aspect ratios, (a) 1.67 and (b) 0.84, after recrystallization. The structure with high aspect ratio (a) recovered strain for both Si and Ge. On the other hand, the structure with low aspect ratio (b) exhibits significant strain relaxation, even after recrystallization.

precludes the nucleation of dislocations and the relatively high recrystallization velocities limit mass diffusion and trap point defects, as will be shown in the following section.

V. SIZE-DEPENDENT STRAIN RELAXATION AND ATOMIC MECHANISMS

To quantify the role of size and geometry on strain relaxation, we define the average strain in relaxation in the crystalline region as

$$\text{strain relaxation}\,(\%) = \frac{a_{\mathrm{Ge}} - a_{\mathrm{Si}}}{a^0_{\mathrm{Ge}} - a^0_{\mathrm{Si}}} \times 100, \quad (3)$$

where, a^0_{Ge} and a^0_{Si} are lattice parameters in bulk Ge and Si, respectively. a_{Ge} and a_{Si} are the average lattice parameters for strained Ge and Si layers in the crystalline region obtained from the projected bond distances. Figures 9(a) and 9(b) summarize our MD predictions of average strain relaxation

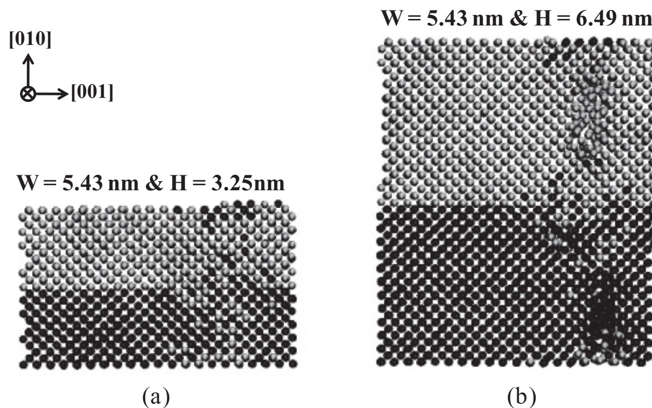

FIG. 8. Atomic snapshots of the structures corresponding to Fig. 7. The high-aspect-ratio structure (a) recovers its original strain state after recrystallization, whereas the low-aspect-ratio structure (b) maintains a fraction of the strain relaxation due to clusters of defects located on either side of the interface.

along the [001] direction as a function of periodic width (W) for various heights (H) of the bilayers before [Fig. 9(a)] and after [Fig. 9(b)] recrystallization. Strain relaxation increases with increasing height of the nanolaminates and decreasing width of the crystal/amorphous regions. Figure 9(b) shows how recrystallization leads to a reduction in the amount of strain relaxation; however, as described above, structures with low aspect ratio retain a significant amount of strain relaxation even after recrystallization.

We now turn to study the atomic origin of strain relaxation. As built, each structure has the same number of Ge atoms on the top half of the simulation cell as Si atoms in the bottom half. During local armophization, high annealing temperature and local melting lead to atomic interdiffusion, leading to a net mass transfer from the originally compressed Ge section into the Si section. Figure 9(c) shows the net number of atoms transported from Ge to Si during local recrystallization per unit volume, and Fig. 9(d) shows the same quantify after recrystallization. A direct relationship between mass transport and strain relaxation is apparent. We find that the net number of atoms translated increases with decreasing width and increasing height as the crystalline Ge expands into the amorphized region and crystalline Si contracts from it. Thus, low-aspect-ratio laminates exhibit more pronounced atomic migration and large strain relaxation. Recrystallization leads to atomic migration in the opposite direction, driven by growth of the Si and Ge lattices. However, this process is not enough to fully reverse the initial atomic migration in low-aspect-ratio structures, and this imbalance in the number of atoms leads to the presence of lattice defects that appear as small clusters [Fig. 8(b)] and are responsible for strain relaxation. We stress again that strain relaxation in this case is not caused by misfit dislocations but by a pair of low-density and high-density defective regions located on either side of the interface. These defects could be long lived at room temperature, making the strain relaxation stable. This cannot, of course, be confirmed or revoked directly with MD simulations because of the short timescales achievable, but MD can test their stability at higher temperatures. We find that even at high temperatures the structures appear stable. At $T = 2000$ K, the strain relaxation in structure with $H = 6.49$ nm and $W = 4.34$ nm does not evolve during the last 200 ps of simulation, and for $H = 6.49$ nm and $W = 5.43$ nm, no strain evolution is observed during the last 500 ps. Accelerated MD techniques[23] could be used to explore the stability of the resulting configuration over longer times.[24]

We now present a simple model that captures the size dependence of the strain relaxation in the amorphized laminates. The average lattice parameters, a_{Ge} and a_{Si}, can be rewritten in terms of the average strain and the bulk lattice parameter as

$$a_{\mathrm{Ge}} = (1 + \langle\varepsilon_{\mathrm{Ge}}\rangle) \cdot a^0_{\mathrm{Ge}} \quad (4)$$

and

$$a_{\mathrm{Si}} = (1 + \langle\varepsilon_{\mathrm{Si}}\rangle) \cdot a^0_{\mathrm{Si}}. \quad (5)$$

Following Park *et al.*,[10] we assume that strain relaxation is complete in a thin region of thickness, W_{rel}, next to the crystal-amorphous interfaces and that the lattice parameters of Si and Ge are the same (i.e., no relaxation) in the interior of

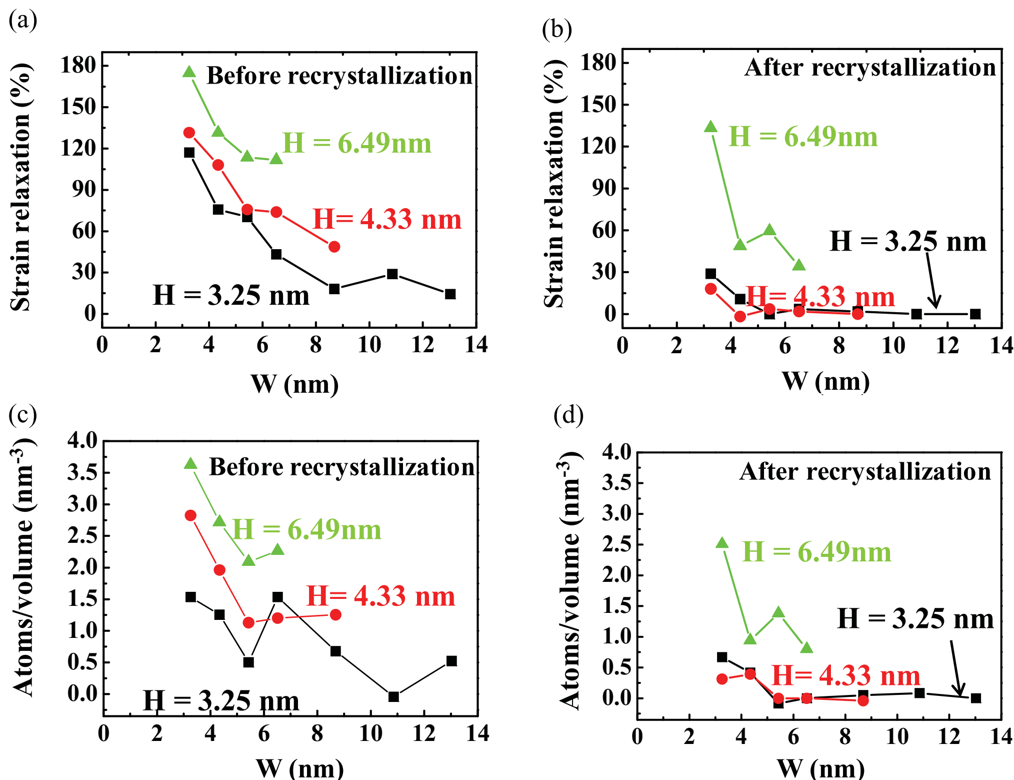

FIG. 9. (Color online) Calculated strain relaxation (a) before and (b) after recrystallization as a function of width for various bilayer height (triangles, $H = 6.49$ nm; circles, $H = 4.33$ nm; squares, $H = 3.25$ nm). The net number of atoms transferred before (c) and after (d) recrystallization.

the crystalline region. The average transverse strains for Ge and Si sections can be then written as

$$\langle \varepsilon_{\mathrm{Ge}} \rangle = -0.0209 + 4 \times 0.0209 \frac{W_{\mathrm{rel}}}{W_0} \tag{6}$$

and

$$\langle \varepsilon_{\mathrm{Si}} \rangle = 0.02 - 4 \times 0.02 \frac{W_{\mathrm{rel}}}{W_0}, \tag{7}$$

Here, W_0 is the original periodic width of the crystalline/amorphous structure, so the crystalline region is considered $W_0/2$. Thus, Eq. (3) can be simply expressed as

$$\text{strain relaxation}\,(\%) = 400.73 \frac{W_{\mathrm{rel}}}{W_0}. \tag{8}$$

As in Park *et al.*,[10] we take W_{rel} to be independent of width and only dependent on height (H) of the nanolaminate. The solid lines in Fig. 10 show the proposed model [Eq. (8)] fitted to our MD data after amorphization (before recrystallization); the resulting W_{rel} values for $H = 3.25$ nm, 4.33 nm, and 6.49 nm are 0.85 nm, 1.03 nm, and 1.40 nm, respectively. As the bilayer height (H) increases, so does the thickness of the strain-relaxed region; the complete strain relaxation region becomes wider, and W_{rel} takes the value of about 1/4 of the bilayer height. This simple model describes the MD results rather well; thus, it could be useful to obtain initial strain relaxation estimates for device design and optimization.

VI. SUMMARY AND CONCLUSIONS

We used molecular dynamic simulations to explore local amorphization followed by recrystallization in epitaxial Si/Ge nanolaminates as an avenue for strain engineering. We find that significant strain relaxation in the crystalline regions can occur in the direction normal to the amorphous/crystalline interface as Ge expands into the amorphous region and Si

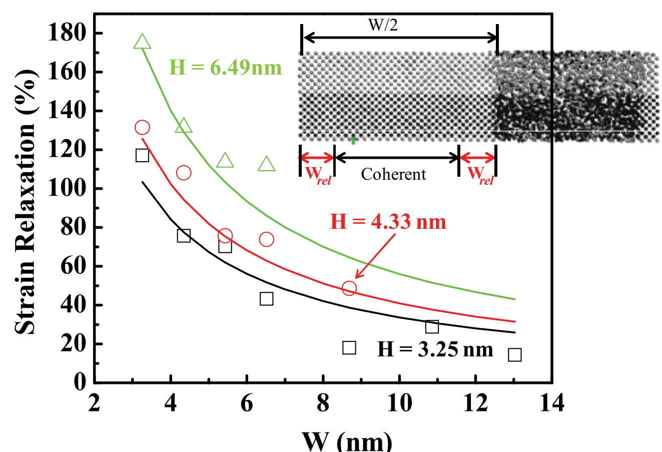

FIG. 10. (Color online) Strain relaxation after amorphization (before recrystallization) for structures with different geometries (triangles, $H = 6.49$ nm; circles, $H = 4.33$ nm; squares, $H = 3.25$ nm). Lines represent the proposed analytical model fitted to the MD data.

contracts from it. The degree of strain relaxation depends on the size and geometry of the Si/Ge heterostructures; strain relaxation increases as the thickness of the Si/Ge bilayer (H) increases or the periodic width (W) of the crystalline/amorphous region decreases. On the basis of the physics revealed by the MD data, we developed a simple model to estimate strain relaxation assuming that thin areas adjacent to the crystalline/amorphous interface are strain-free and the interior Si and Ge sections share the same lattice parameter. This simple model shows good agreement with our MD results; thus, it can be used for an initial estimate of strain relaxation for a given geometry. After recrystallization, some of the strain relaxation is lost; however, structures with low aspect ratios are able to retain a significant fraction of the strain relaxation in their crystalline regions. Interestingly, strain relaxation in these structures happens with coherent interfaces with no misfit dislocations and is caused by point defect clusters on either side of the interface.

Our results show that amorphization followed by recrystallization is a promising avenue for strain engineering of heterostructures for nanoelectronic applications. Therefore, the size and geometry of the nanostructure can be optimized for local amorphization and recrystallization to result in two possible outcomes: (i) a recovery of the initial strain state (this is desirable in nanostructures in which the desired strain state has already been engineered) and (ii) uniaxial strain relaxation for improved electronic properties.

ACKNOWLEDGMENT

This work was supported by the Microelectronics Advanced Research Corporation and its Focus Center on Materials, Structures, and Devices, by the Network for Computational Nanotechnology through nanoHUB.org computational resources funded by the US National Science Foundation Grant No. EEC-0228390.

[*]strachan@purdue.edu

[1]K. Brunner, Rep. Prog. Phys. **65**, 27 (2002).

[2]J. P. Zhang, R. J. Wilson, P. L. F. Hemment, A. Claverie, F. Cristiano, P. Salles, J. Q. Wen, J. H. Evans, A. R. Parker, and G. J. Parker, Nucl. Instr. And Meth. B **84**, 222 (1994).

[3]M. Ishimaru, M. Yamaguchi, and Y. Hirotsu, Jpn. J. Appl. Phys. **43**, 7966 (2004).

[4]S. Yamaguchi, N. Sugii, S. K. Park, K. Nakagawa, and M. Miyao, J. Appl. Phys. **89**, 2091 (2001).

[5]J. H. Haeni, P. Irvin, W. Chang, R. Uecker, P. Reiche, Y. L. Li, S. Choudhury, W. Tian, M. E. Hawley, B. Craigo, A. K. Tagantsev, X. Q. Pan, S. K. Streiffer, L. Q. Chen, S. W. Kirchoefer, J. Levy, and D. G. Schlom, Nature **430**, 758 (2004).

[6]Z. Xu and M. J. Buehler, Nanotechnology **20**, 185701 (2009).

[7]S. E. Thompson, M. Armstrong, C. Auth, S. Cea, R. Chau, G. Glass, T. Hoffman, J. Klaus, Z. Ma, B. Mcintyre, A. Murthy, B. Obradovic, L. Shifren, S. Sivakumar, S. Tyagi, T. Ghani, K. Mistry, M. Bohr, and Y. El-Mansy, IEEE Electron. Device Lett. **25**, 191 (2004).

[8]I. Åberg, C. N. Chléirigh, and J. L. Hoyt, IEEE Trans. Electron Devices **53**, 1021 (2006).

[9]P. Hashemi, L. Gomez, J. L. Hoyt, M. D. Robertson, and M. Canonico, Appl. Phys. Lett. **91**, 083109 (2007).

[10]Y. Park, H. M. Atkulga, A. Grama, and A. Strachan, J. Appl. Phys. **106**, 034304 (2009).

[11]M. Lee, E. A. Fitzgeeald, M. T. Bulsara, M. T. Currie, and A. Lochtefeld, J. Appl. Phys. **97**, 011101 (2005).

[12]H. Yin, Z. Ren, K. L. Saenger, H. J. Hovel, J. P. de Souza, J. A. Ott, R. Zhang, S. W. Bedell, G. Pfeiffer, R. Bendernagel *et al.*, in *8th International Conference on Solid-State and Integrated Circuit Technology* (ICSICT, Shanghai, 2006), pp. 136–138.

[13]A. C. T. van Duin, A. Strachan, S. Stewman, Q. Zhang, X. Xu, and W. A. Goddard III, J. Phys. Chem. A **107**, 3803 (2003).

[14]M. J. Buehler, A. C. T. van Duin, and W. A. Goddard, Phys. Rev. Lett. **96**, 095505 (2006).

[15]D. Sen, C. Thaulow, S. V. Schieffer, A. Cohen, and M. J. Buehler, Phys. Rev. Lett. **104**, 235502 (2010).

[16]J. C. Berendsen, J. P. M. Postma, W. F. van Gunsteren, A. Di Nola, and J. R. Haak, J. Chem. Phys. **81**, 3684 (1984).

[17]A. Mattoni and L. Colombo, Phys. Rev. B **69**, 045204 (2004).

[18]G. L. Olsen and J. A. Roth, Mater. Sci. Rep. **3**, 1 (1988).

[19]B. C. Johnson, P. Gortmaker, and J. C. McCallum, Phys. Rev. B **77**, 214109 (2008).

[20]C. Krzeminski, Q. Brulin, V. Cuny, E. Lecat, E. Lampin, and F. Cleri, J. Appl. Phys. **101**, 123506 (2007).

[21]E. J. Albenze and P. Clancy, Mol. Simul. **31**, 11 (2005).

[22]M. Posselt and A. Gabriel, Phys. Rev. B **80**, 045202 (2009).

[23]A. F. Voter, F. Montalenti, and T. C. Germann, Annu. Rev. Mater. Res. **32**, 321 (2002).

[24]T. Ichinomiya, B. P. Uberuaga, K. E. Sickafus, Y. Nishiura, M. Itakura, Y. Chen, Y. Kaneta, and M. Kinoshita, J. Nucl. Mater. **384**, 315 (2009).